INTERNATIONAL JOURNAL OF INTEGRATED ENGINEERING
ISSN: 2229-838X e-ISSN: 2600-7916

IJIE

Vol. 17 No. 7 (2025) 274-286
https://publisher.uthm.edu.my/ojs/index.php/ijie

Damage Evaluation of Corroded Reinforced Concrete Beam Based on Acoustic Emission Signal Strength

Khairul Anuar Shahid[1]*, N. Muhamad Bunnori[2], Mohd Khairul Kamarudin[3]

[1] *Faculty of Civil Engineering Technology,*
Universiti Malaysia Pahang Al-Sultan Abdullah, 26300 Kuantan, Pahang, MALAYSIA
[2] *Faculty of Engineering,*
University of Malaya, 50603 Kuala Lumpur, MALAYSIA
[3] *School of Civil Engineering,*
Universiti Teknologi MARA, 40450 Shah Alam, Selangor, MALAYSIA

*Corresponding Author: khairulanuars@umpsa.edu.my
DOI: https://doi.org/10.30880/ijie.2025.17.07.026

Article Info

Received: 19 February 2025
Accepted: 28 August 2025
Available online: 31 December 2025

Keywords

Acoustic emission, corrosion monitoring, signal strength, simplified cyclic load test, damage evaluation

Abstract

An acoustic emission (AE) technique has been employed to monitor crack damage in various initial conditions of corroded reinforced concrete beams subjected to a simplified cyclic load test (SCLT). Limited studies have assessed the validity of AE techniques for corroded reinforced concrete structures, particularly in full-scale specimens. This study aimed to explore damage evaluation techniques based on the AE signal strength parameter. The beam specimens were exposed to a 45-day corrosion process, with corrosion accelerated using the impressed current technique. The results obtained were then compared to those of the control specimen. The AE signal strength data analysis revealed that the signal strength parameter is consistent with visual observation (crack mapping) during SCLT. Additionally, the presence of corrosion in the reinforced concrete beam reduced the signal strength because fewer cracks formed in the corroded specimen. Therefore, the analysis of the AE signal strength parameter seems promising for non-destructive evaluation in structural health monitoring.

1. Introduction

Reinforced concrete (RC) is one of the most widely used materials in the construction industry, encompassing a diverse range of applications, from buildings and bridges to dam structures. The combination of steel reinforcement and the concrete itself enhanced the mechanical properties of the reinforced concrete in terms of tensile and compressive strength. However, due to excessive load, environmental distress, or earthquakes, the reinforced concrete is prone to deterioration during its service life.

Corrosion of steel in concrete is said to be the leading cause, which can lead to a loss of strength due to a reduction in the steel's area within the concrete. In Malaysia, most highway bridges, especially those constructed with concrete, with a service life of more than 40 years, suffer from deterioration issues. According to the Public Works Department of Malaysia [1], more than 400 bridges in Malaysia were categorised as critical due to deterioration in 2007. As a result, 3.7 million USD was spent on bridge repair and maintenance works in the same year. This is alarming for the country, where a significant portion of the budget must be allocated to provide good service to road users. With a limited budget and a high number of critical bridges, prioritisation of maintenance and repair work is essential. Therefore, early detection of corrosion can reduce maintenance costs, thereby prolonging the service life of a bridge through effective structural health monitoring (SHM).

Structural health monitoring refers to the implementation of a damage identification strategy for civil engineering infrastructures, so that any damage to the structure can be detected early [2]. The primary advantage of SHM is the support in decision-making concerning the determination of priorities for maintenance and repair work. Additionally, the demand for maintenance and repair work can be estimated effectively over the entire life cycle of the structure with the availability of assessment data. Rapid development in electronic and sensor technology has indirectly contributed to the application of NDT methods in SHM. Generally, NDT methods for SHM do not cause any damage to the targeted structure during testing. Zaki et al. [3] has categorised the NDT methods for corrosion monitoring and detection based on their principles, such as electrochemical, electromagnetic, and elastic wave methods.

The AE technique is among the most popular NDT methods used for the structural health monitoring of civil engineering infrastructures. The fundamental concept of the AE technique is based on wave theory, stating that bursting or rapid energy release arises from a localised source within a material and produces elastic stress waves known as acoustic emission waves [4]. The effectiveness of AE technology in the monitoring and assessment of damage in reinforced or post-tensioned concrete has been considerably investigated [5]–[8]. Kaphle [9] stated that the key advantage of the AE technique is its high sensitivity in detecting cracks and damage, so the cracks can be detected at the early stages of damage. Webb et al. [10] performed a case study to evaluate the performance of the monitoring system of prestressing tendon wire breaks on Hammersmith Flyover, located in central London. They suggested that the use of an AE technique greatly contributes to visual inspection for targeting the location of corrosion. Therefore, the presented evidence can justify the effectiveness of AE techniques in global bridge monitoring.

Valuable AE parameters for AE data analysis are signal strength and cumulative signal strength. The term signal strength typically refers to the area under the voltage signal of AE throughout the waveform. ASTM [11] defined signal strength as "the measured area of a rectified AE signal with the unit proportional to volt-second". The determination of signal strength normally includes the absolute area of the positive and negative areas, as suggested by Ziehl & Ridge [12]. In general, the fundamental purpose of signal strength analysis is to serve as a rational damage indicator, as it provides a measure of the waveform energy released by the specimen.

The AE signal strength can be used for evaluating damage in reinforced concrete structures. Md Nor et al. [13] conducted an experiment on fatigue damage to a reinforced concrete beam and analysed monitoring data by using AE signal strength. They discovered that a spike in signal strength could be linked to the initiation and propagation of cracks. Mangual et al. [14] used cumulative signal strength to characterise the corrosion stages on corroded prestressed concrete and found that a drastic increase in cumulative signal strength is associated with the nucleation of wide tensile cracks. In other words, the cumulative signal strength increases when damage severity exacerbates. Several methods have been developed to evaluate AE data in corroded reinforced concrete structures, which involve the early detection and quantification of corrosion, the detection of crack damage, the classification of crack damage, the evaluation of crack damage severity, and the localisation of crack damage sources.

The previous studies on corroded reinforced concrete using the AE technique, however, have only focused on small-scale specimens [15]–[18]. Therefore, there is a need for the structural performance evaluation of full-scale reinforced concrete beams whose structural behaviour is likely to differ from that of the small-scale specimens. Additionally, the use of the AE technique for damage evaluation is promising due to its sensitivity to internal damage, which can correlate well with mechanical loads or any damage to the concrete. This study reports on an experimental study using the AE technique to identify damage, utilising the AE signal strength parameter analysis on the corroded full-scale reinforced concrete specimens.

2. Methodology

2.1 Material and Specimen Preparation

Four precast reinforced concrete beams with a dimension of 300 mm × 600 mm × 4050 mm were cast in a yard at OKA Concrete Sdn Bhd in Bukit Selambau, Sungai Petani, Kedah. Full-scale beam specimens were selected to assess the actual structural performance of the beam under conditions of corrosion and loading. The specimen was designed in accordance with EN 1992: Eurocode 2 - Design of Concrete Structures [19]. The details of the specimen are illustrated in Fig. 1. The beam specimens were cast using concrete grade 40, and the concrete was proportioned with a cement: sand: aggregate: water ratio of 1:2.45:2.87:0.44. A superplasticiser (3.55 L) was added to the concrete mix to improve its workability. The type of aggregate used in the mix was crushed single-sized granite with a maximum size of 20 mm. For reinforcements, the nominal diameter of bars used for compression is T12, whereas the nominal diameter of bars used for tension is H16, respectively. A stirrup of size 8 mm was used as shear links, spaced 250 mm centre-to-centre. The concrete cover was designed to be 40 mm thick, based on Eurocode 2: Design of Concrete Structures [19], to mitigate chloride-induced corrosion from seawater. One pristine specimen was used as a control, and three specimens were exposed to different durations

Int. Journal of Integrated Engineering Vol. 17 No. 7 (2025) p. 274-286

of corrosion experiments. One of the tension steel bars for each specimen was designed to be exposed from the concrete for half-cell potential measurement and accelerated corrosion experiment. To label the specimen, "XY-T" format was used where "X" indicates corrosion conditioning ("C" for conditioning and "U" is unconditioning), "Y" indicates the specimen condition ("U" for uncracked and "C" for pre-cracked specimen), "T" and followed by a number indicates the duration of the accelerated corrosion conditioning; for example, CU-T45 means corroded uncracked with 45 days of corrosion conditioning. The control specimen was labelled as CTRL.

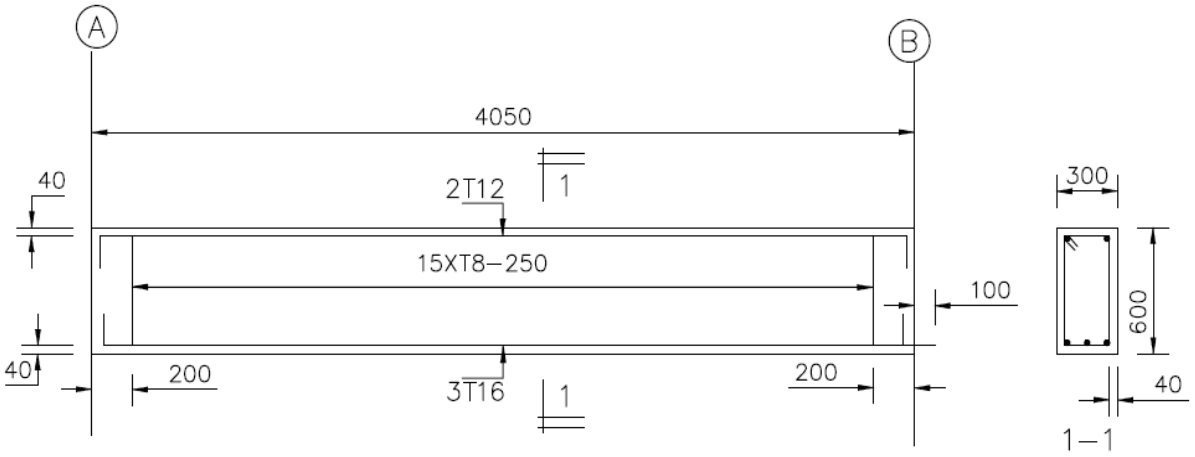

Fig. 1 *Specimen detailing (all units in mm)*

2.2 Accelerated Corrosion Experiment

Three beams were subjected to an accelerated corrosion process by using the impressed current technique with different corrosion durations. The impressed current technique was employed to accelerate the reinforcement corrosion by applying an electrochemical potential between the steel reinforcing bar (anode) and a copper plate (cathode), as illustrated in Fig. 2. The beam specimens were partially immersed in a 3.5% NaCl solution to simulate the marine environment in the laboratory. Before electrolysis was carried out, a copper wire was used to connect the steel reinforcing bar (anode) to the positive terminal of a direct current (DC) power supply. DC's negative terminal was connected to a copper plate (cathode) via the copper wire. A constant current density of 100 mA/cm^2, which is the maximum current density occurring under natural conditions [20], was applied to accelerate the corrosion. The duration of the accelerated corrosion experiment varied from 15 to 45 days. The description of the specimens is summarised in Table 1. After the corrosion test had been completed, all specimens were tested under a 4-point bending setup.

Fig. 2 *Experimental setup for accelerated corrosion test using an impressed current technique*

2.3 Simplified Cyclic Load Test Procedure

The CLT procedure was proposed by the ACI 437 committee and briefly described in ACI 437.1R-12 [21]. This method is considered an improved and economical alternative to monotonic load tests [22]. CLT is based on a concentrated load applied to a specimen by using a hydraulic jack system. CLT also consists of a series of load sets, each of which includes two identical load cycles. Each load cycle involves five load steps. The purpose of using

identical load cycles is to evaluate the system's permanence and repeatability. Another evaluation criterion that needs to be checked is DFL derived from a stepped loading pattern.

The minimum number of load sets is three, where the first load set should not exceed the service load level or 50% of the expected total test load. The second load set is conducted in a manner similar to the first load set, but with an applied load approximately halfway between the first load set and the total test load. The final load set is carried out similarly to the previous load set, and the applied load is the same as the total test load. Liu [23] recommended a total test load of at least 85% of the ultimate load test and a minimum holding load of at least 10% of the total test load. A typical loading profile of CLT is shown in Fig. 3.

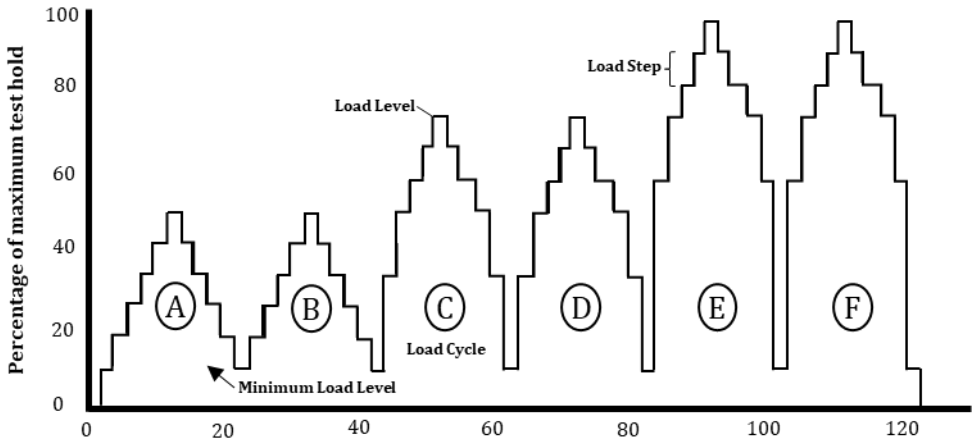

Fig. 3 *Schematic load profile of CLT per ACI 437 [21]*

In this study, all specimens underwent a simplified cyclic load test (SCLT), with the applied load varying according to the degree of corrosion applied. The test consisted of a series of load sets, each with an identical load cycle named C1 and C2. The SCLT did not contain any load steps, as introduced in a normal CLT method, as shown in Fig. 4. Consequently, the load was ramped to the desired level at a constant rate. The SCLT procedure was applied by Shahidan [24] as part of an experimental program to study the damage in reinforced concrete. The maximum test load should be at least 85% of the ultimate capacity, whereas the first load set should not exceed 50% of the total test load. The minimum holding load should be at least 10% of the test load [23]. The holding period at the top of each load cycle and the minimum load cycle was 3 min. The minimum holding load was 30 kN throughout the test to keep the actuator engaged. The simplified cyclic load test consisted of eight load sets (16 load cycles). The load applied to the specimens is shown in Table 1. After the SCLT was completed, all of the specimens were loaded until failure occurred to determine their ultimate capacity.

During the SCLT and AE monitoring, the development of cracks was observed. The visible cracks were marked, and their width was measured using a crack comparator. The visible cracks were marked according to the phases of the loading. During this period, the AE monitoring system was paused to prevent any unwanted signals from being recorded. To reduce the AE signal noise, the neoprene pad was placed between the beam and the reaction stands.

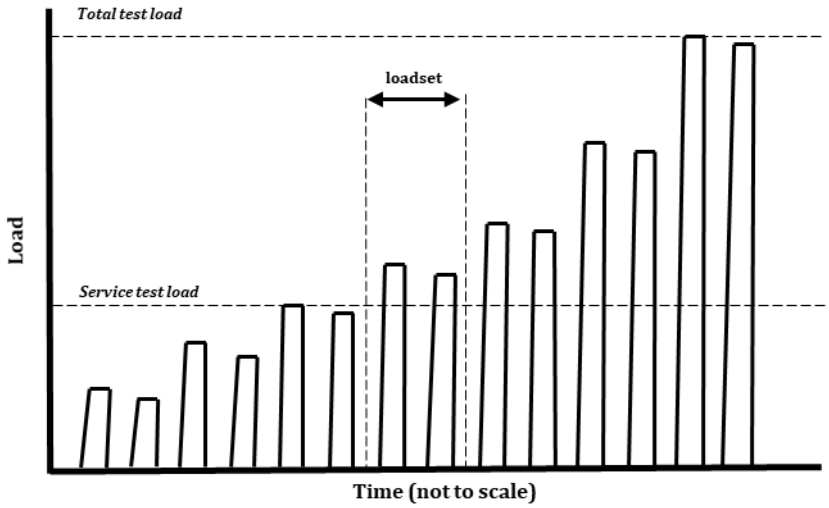

Fig. 4 *Simplified cyclic load test (SCLT) [12]*

Int. Journal of Integrated Engineering Vol. 17 No. 7 (2025) p. 274-286

Table 1 *Applied load levels for each specimen based on ultimate capacity (Pu)*

Specimen	LS1	LS2	LS3	LS4	LS5	LS6	LS7	LS8	Ultimate Load (Pu) kN
CRTL	0.18 Pu	0.27Pu	0.37Pu	0.46Pu	0.55Pu	0.64Pu	0.73Pu	0.82Pu	361.3
CU-T45	0.21Pu	0.31Pu	0.41Pu	0.52Pu	0.62Pu	0.72Pu	0.83Pu	0.93Pu	300.4

To assess the crack damage, the AE analysis was carried out based on the application of AE signal strength. In each phase of the loading, the signal strength parameter was plotted against time and normalised load. The normalised load was calculated based on the ratio between the applied load and the ultimate load for each specimen. The analysis was based on AE signal strength versus time and cumulative signal strength versus time. In this analysis, AE signal strength data were collected from all sensors. This is because the visible cracks appeared from sensor 1 to sensor 6. Moreover, the transition pattern of cracks from flexural to shear can be identified based on this arrangement. Fig. 5 shows the arrangement of the AE sensors on the reinforced concrete specimen. The horizontal distance between the AE sensors is 300 mm. Meanwhile, the vertical distance is 200 mm (from the bottom) for S1 to S4 and 150 mm (from the bottom) for S5 and S6, respectively.

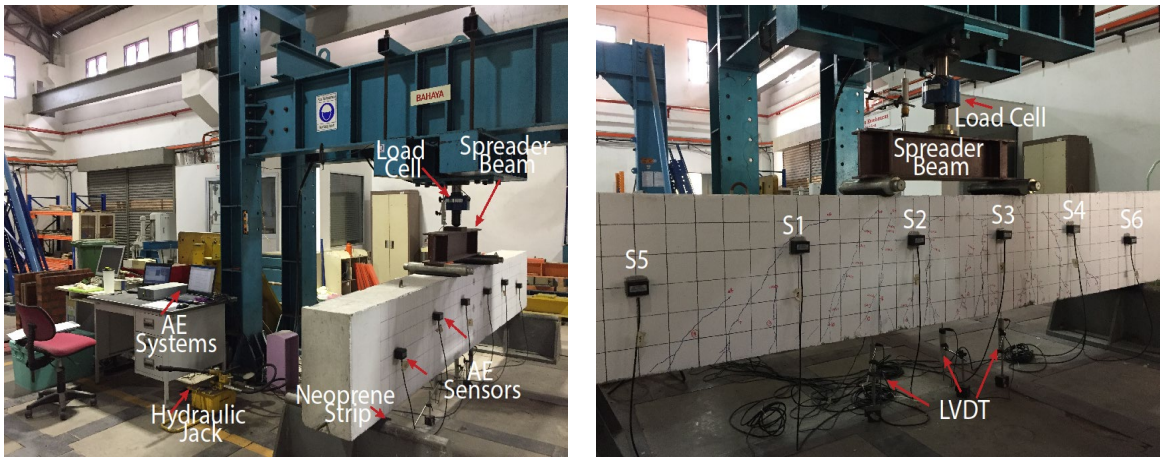

Fig. 5 *Experimental setup for CLT and AE monitoring*

2.4 Acoustic Emission Monitoring

A Physical Acoustic Corporation (PAC) type R6I-AST sensor with a resonance frequency of approximately 55 kHz was used throughout the test, featuring an integral 40 dB pre-amplifier. The sensor was mounted to the surface of the concrete using steel plates attached with two-part epoxy resin. Industrial grease was used between the concrete surface and the sensors to enhance the electrical connection and reduce friction between the two surfaces. The AE sensors were then connected to the 8-channel acquisition system (PCI-8 AE System, Mistras Group Inc.) for data collection. Pencil Lead Fracture (PLF) is used for verifying sensor mounting. The technique imitates the same fundamentals of AE source with standards to comply with procedures stipulated in ASTM E976-10 [4]. The specimens subjected to CLT were monitored continuously using the AE system.

Before the commencement of AE monitoring, system timing parameters, including Peak Definition Time (PDT), Hit Definition Time (HDT), and Hit Lockout Time (HLT), were set at 1000, 2000, and 500 µs, respectively. For the waveform setup, the sample rate was 1 MPSP with a pre-trigger at 250 µs, and the data length was 1 k. The threshold level was set at 45 dB based on the result obtained from the noise test to eliminate electrical and mechanical noises generated during monitoring. The threshold limit filtered out unwanted noise from the surrounding environment, which was determined based on the noise test results. Md Nor et al. [25] applied the same threshold value and amplitude range to study the fatigue damage test of the reinforced concrete beam using the AE technique.

The friction between the beam specimens and the support during the four-point bending test could generate noise. Therefore, to minimise noise intervention during the test, neoprene strips were placed on both supports. A similar action was taken by Abdelrahman et al. [26] as part of mitigation action during a cyclic load test on a reinforced concrete beam using the AE technique. The neoprene strips were installed at the two rollers that attached to the spreader beam and at the two supports, as depicted in Fig. 5.

2.5 AE Signal Strength Damage Evaluation

2.5.1 Signal Strength and Cumulative Signal Strength

In the literature, the term signal strength typically refers to the area under the voltage signal of AE throughout the waveform. In general, the fundamental purpose of signal strength analysis is to serve as a rational damage indicator, as it provides a measure of the waveform energy released by the specimen. Md Nor et al. [27] have experimented with fatigue damage to reinforced concrete beams and further analysed the monitoring data using AE signal strength. It was observed that higher signal strength was developed at the early onset of cracks. An analysis using cumulative signal strength to characterise the corrosion stages is performed by Mangual et al. [28] on corroded pre-stressed concrete. Based on the analysis, it was found that a drastic increase in cumulative signal strength was associated with the nucleation of wide tensile cracks. In other words, the cumulative signal strength is increased when the severity of damage is increased.

2.5.2 CSS Load Ratio

The CSS load was studied by Ziehl & Ridge [12] and they discovered that the ratio of cumulative signal strength during reloading to that during the initial loading could be an indicator of damage in reinforced concrete. They have established the maximum value of 40% for the CSS load ratio as the acceptance criterion based on their experimental analysis. In other words, when the CSS load ratio is less than 40%, the tested specimen is acceptable and not significantly damaged. Besides, the safety margin based on this criterion yields a better result compared to the CLT evaluation criterion. However, this ratio is more effective for moderate to heavy damage. The CSS load ratio is calculated by dividing the CSS measured during reloading by the CSS measured during initial loading.

3. Results and Discussion

3.1 Crack Observation

Fig. 6 shows the crack mapping of the beam specimen under the eight phases of load sets. Since the visible crack begins to appear at LS3 for both specimens, the mapping is only shown from LS3 to LS8, as represented in Fig. 6(a) to Fig. 6(f) for the CTRL specimen and Fig. 6(g) to Fig. 6(l) for the CU-T45 specimen. At LS3, five cracks appeared on the specimen's surface, approximately between sensors 1 and 4, as shown in Fig. 6(a). The average crack mouth opening displacement (CMOD) is 0.15 mm. In contrast, there were seven cracks that appeared on the surface of the CU-T45 specimen, as shown in Fig. 7(g). The crack at the mid-span of the beam was propagated vertically beyond the neutral axis for both specimens, and most of the cracks had 0.2 mm CMOD. According to McCormac & Nelson [29], the reinforcing bars inside the beam have yielded if the cracks occur beyond the neutral axis.

For the CTRL specimen, six more vertical cracks appeared on the surface of the concrete in LS4. The rest of the cracks were just propagated from the tip of the preceding crack. At LS5, three more new vertical cracks appeared on the surface of the specimen in the shear region on both sides of the specimen. Interestingly, the previous cracks that appeared at the constant moment region have stopped developing. At LS6, two more cracks appeared on the surface of the specimen in the shear region and diagonal in their pattern and propagated beyond the neutral axis when 64% of the ultimate load was applied. There was no new crack that appeared on the surface of the concrete when the specimen was subjected to LS7 and LS8.

For the CU-T45 specimen, two more vertical cracks appeared in LS4. Only one diagonal crack appeared on the surface of the concrete in LS5 when 62% of the ultimate load was applied. The rest of the cracks were just propagated from the tip of the preceding crack. At LS6, two more cracks appeared, while in LS7, three more cracks appeared in the shear region. All of them were diagonal in shape and propagated towards the previous vertical cracks. There were no new cracks that appeared in the LS8. It was observed that the number of cracks in the corroded specimen was fewer compared to the control specimen, which is in agreement with the findings of Zaki et al. [16], who reported a lower number of cracks in the highly corroded specimen. This result may be due to the deterioration of the bonding between the steel reinforcement and concrete caused by corrosion products, which affected the stress distribution within the beam specimen when the flexural load was applied. It was also noticed that shear cracks appeared in LS5 for corroded specimens, which happened earlier than in the control specimen.

Table 2 shows the crack mouth opening displacement for the CTRL specimen. On average, the crack width for the first 5 flexural cracks in load set 3 was 0.155 mm, which has been categorised as a narrow crack based on the Road Engineering Association of Malaysia (REAM) [30]. Most of these cracks remained active from load set 3 until the ultimate load phase. At the ultimate load, four of the cracks have recorded a crack width of more than 2.5 mm, which was categorised as a wide crack. At load set 4, the average crack width for the six new cracks was 0.1 mm, which also falls under the narrow crack category; some of them remained active until load set 8. At load sets 5 and 6, five additional new cracks formed, and most of these cracks occurred outside the constant moment region. Most of these cracks were diagonal in shape and remained active until the final load was applied, with a crack width

Int. Journal of Integrated Engineering Vol. 17 No. 7 (2025) p. 274-286

exceeding 0.35 mm. However, all these cracks were categorised as medium cracks when the specimen was subjected to the ultimate load.

Table 3 shows the crack mouth opening displacement for the CU-T45 specimen. At load set 3, seven cracks have appeared on the surface of the concrete, with an average crack width of approximately 0.17 mm. The number of cracks was higher at this load set compared to the CTRL specimen, and all cracks remained active until the final load set. Later, only two new cracks were formed at load set 4, one at load set 5, and two at load sets 6 and 7, respectively. In the shear region, cracks began to form approximately between load set 4 and load set 5, continuing until the final load set. These cracks actively propagated in terms of both crack width and length in load sets 6 and 7, especially for crack 12, which experienced a dramatic increase in crack width from 0.1 mm to 0.55 mm.

A comparison of the results between the control and corroded specimens, based on crack width opening displacement, revealed that the corroded specimen recorded a significantly wider crack width, especially in the constant moment region where the corrosion test was conducted. Although the number of cracks formed in the corroded specimen was fewer compared to the control specimen, the crack width was wider, with three cracks recorded, measuring 4.0 mm in width, compared to 2.5 mm for the control specimen. These results are likely to be affected by the accumulation of corrosion products (oxides), which reduce the bonding between the steel bar and the concrete. Corrosion also affects the tensile behaviour of the steel bar by reducing the cross-sectional area of the bar. As such, the load-carrying capacity of the bars is reducing, and these effects on the tensile behaviours of the bar could be significant [31]. Therefore, the crack width for flexural cracks is wider in the corroded specimen.

Interestingly, shear cracks in the shear region have been propagated rapidly towards the two-point loads in LS6 for both specimens. In the constant moment region, no crack development occurred. However, in the shear region, most of the cracks were propagated rapidly from the tip of the previous cracks towards the two-point loads. In other words, the flexural crack becomes inactive when more shear cracks are formed. In LS8, however, the vertical crack starts to propagate again towards the upper area of the specimen in the constant moment region. In the shear region, the cracks were propagated diagonally from the tip of the previous crack towards the two-point loads, and some of the small cracks developed and finally joined with the main crack, as shown in Fig. 6(f) to Fig.6(l).

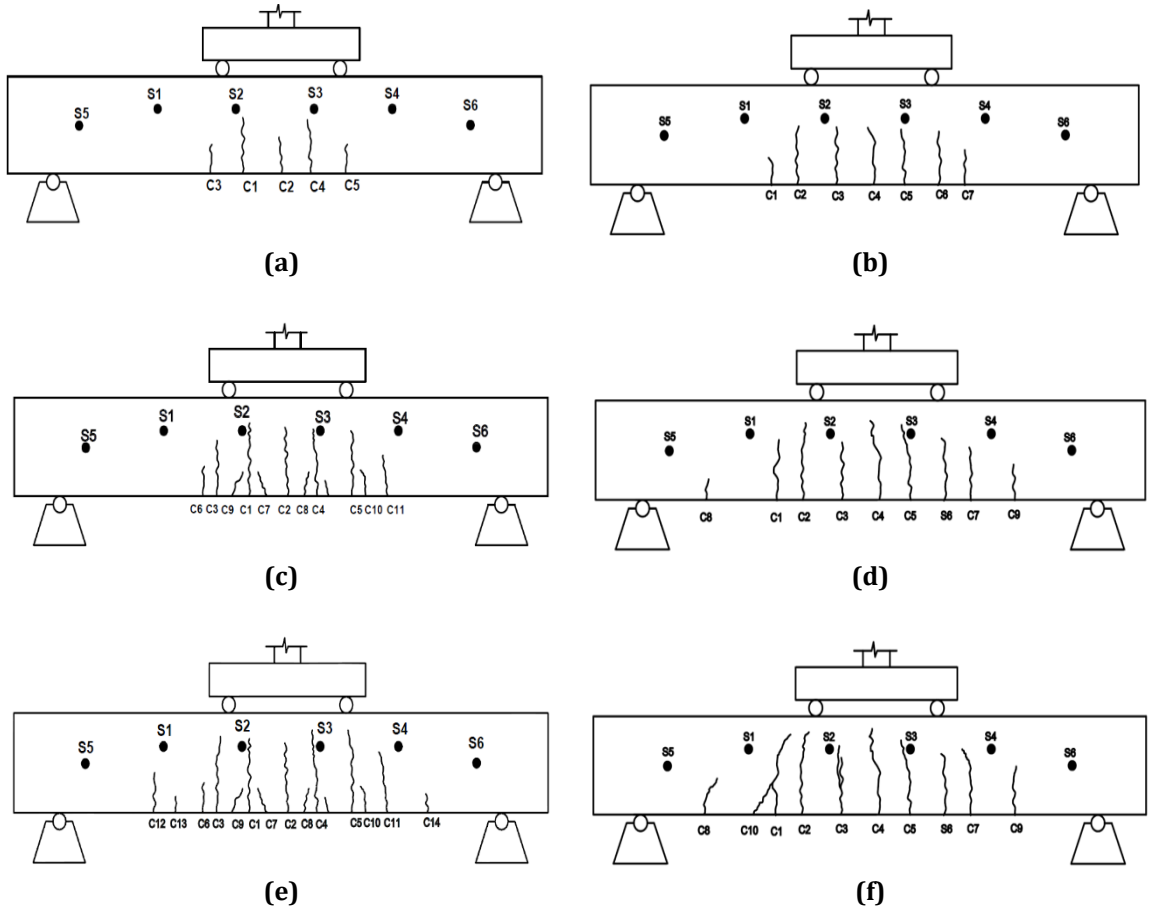

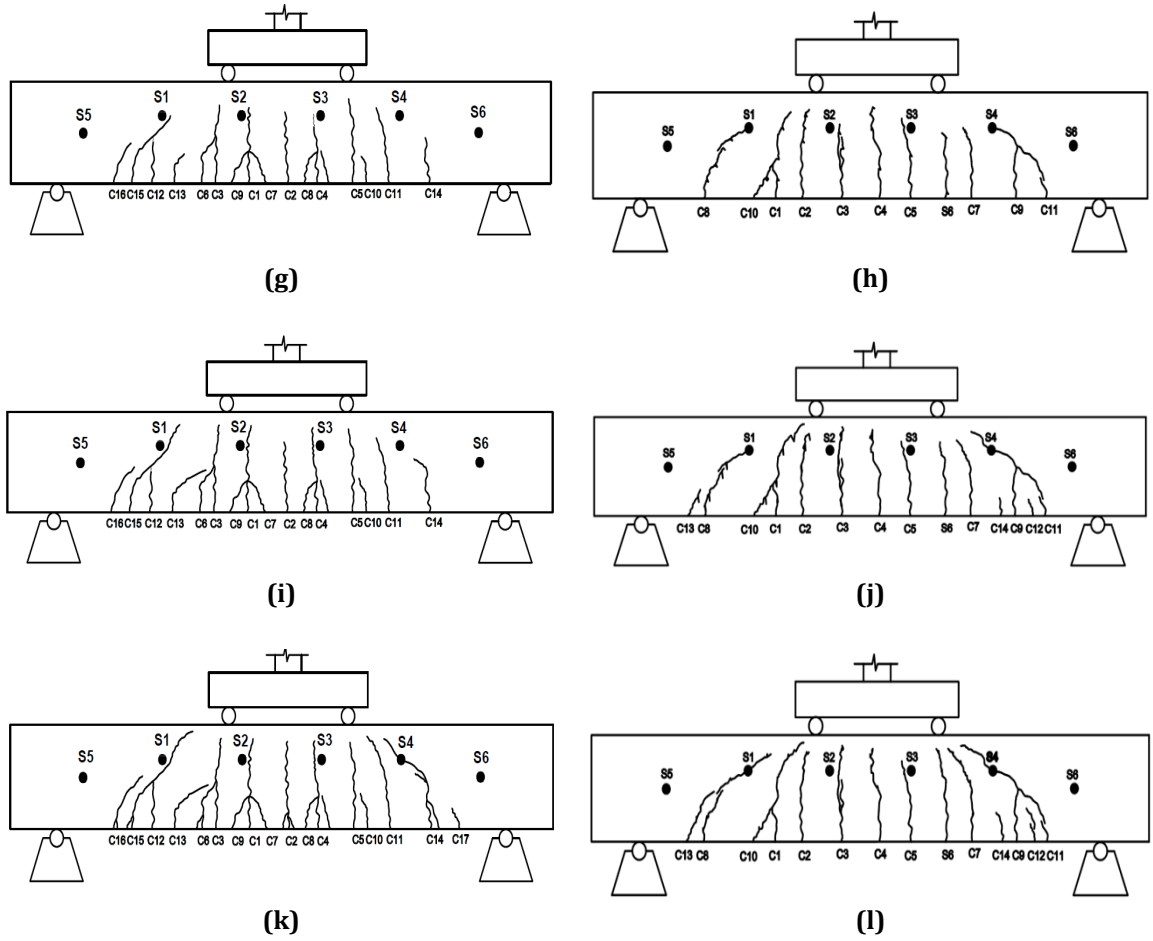

Fig. 6 *Crack mapping for (a)-(f) Specimen CTRL; and (g)- (l) Specimen CU-T45*

Table 2 *Crack mouth opening displacement (CMOD) for CTRL specimen*

	LS1		LS2		LS3		LS4		LS5		LS6		LS7		LS8		Pu
Crack	C1	C2	C1	C2	C1	C2	C1	C2	C1	C2	C1	C2	C1	C2	C1	C2	
1					0.2	0.25	0.3	0.3	0.4	0.4	0.45	0.45	0.45	0.55	0.55	0.65	2.5
2					0.15	0.15	0.2	0.25	0.3	0.35	0.35	0.35	0.35	0.35	0.4	0.4	2.5
3					0.1	0.1	0.1	0.1	0.2	0.2	0.25	0.25	0.4	0.4	0.5	0.5	0.5
4					0.15	0.15	0.2	0.25	0.3	0.4	0.4	0.4	0.4	0.4	0.45	0.5	3
5					0.15	0.15	0.2	0.3	0.35	0.4	0.4	0.45	0.45	0.5	0.5	0.6	2.5
6							0.1	0.1	0.2	0.2	0.25	0.4	0.4	0.4	0.45	0.5	0.5
7							0.1	0.1	0.15	0.15	0.15	0.15	0.2	0.2	0.2	0.3	0.35
8							0.1	0.1	0.15	0.15	0.3	0.35	0.35	0.4	0.4	0.4	1.5
9							0.1	0.1	0.15	0.15	0.15	0.15	0.15	0.2	0.2	0.2	0.25
10							0.1	0.1	0.15	0.15	0.2	0.2	0.2	0.25	0.25	0.35	0.8
11							0.1	0.1	0.15	0.15	0.35	0.35	0.4	0.45	0.45	0.55	0.6
12									0.1	0.1	0.2	0.2	0.2	0.25	0.3	0.35	0.45
13									0.1	0.1	0.1	0.15	0.2	0.25	0.3	0.4	0.45
14									0.1	0.1	0.15	0.15	0.2	0.2	0.5	0.55	0.7
15											0.1	0.1	0.45	0.55	0.65	0.75	0.85
16											0.1	0.1	0.25	0.35	0.5	0.5	0.75

* All units in mm

* C1 and C2 represent Cycle 1 and Cycle 2

Int. Journal of Integrated Engineering Vol. 17 No. 7 (2025) p. 274-286

Table 3 *Crack mouth opening displacement (CMOD) for CU-T45 specimen*

	LS1		LS2		LS3		LS4		LS5		LS6		LS7		LS8		Pu
Crack	C1	C2	C1	C2	C1	C2	C1	C2	C1	C2	C1	C2	C1	C2	C1	C2	
1					0.1	0.1	0.15	0.25	0.3	0.35	0.45	0.45	0.5	0.5	0.65	0.65	0.7
2					0.2	0.25	0.35	0.4	0.4	0.45	0.5	0.55	0.7	0.7	0.8	0.85	0.85
3					0.2	0.25	0.25	0.4	0.5	0.55	0.6	0.6	0.65	0.7	0.8	0.9	4
4					0.2	0.25	0.3	0.35	0.45	0.45	0.5	0.6	0.65	0.7	0.85	0.9	4
5					0.2	0.25	0.3	0.35	0.4	0.45	0.6	0.6	0.65	0.75	0.9	1	4
6					0.2	0.3	0.35	0.4	0.5	0.55	0.65	0.65	0.7	0.8	0.8	0.9	0.9
7					0.1	0.1	0.2	0.35	0.35	0.4	0.45	0.5	0.55	0.55	0.55	0.7	0.7
8								0.1	0.1	0.15	0.15	0.15	0.2	0.2	0.35	0.5	0.5
9								0.1	0.1	0.3	0.4	0.4	0.45	0.45	0.45	0.45	0.5
10									0.2	0.3	0.45	0.45	0.5	0.5	0.55	0.6	0.65
11											0.1	0.1	0.2	0.35	0.4	0.45	0.5
12												0.1	0.55	0.55	0.65	0.7	0.75
13													0.1	0.3	0.35	0.45	0.55
14														0.1	0.35	0.4	0.45

* All units in mm

* C1 and C2 represent Cycle 1 and Cycle 2

3.2 AE Signal Strength Parameter

Fig. 7 shows the trend of AE signal strength parameters corresponding to different levels of normalised load over time for the CTRL and CU-T45 specimens. In the LS1 and LS2, few signals have been recorded due to the formation of microcracks in both specimens. In the LS3, macrocracks (visible cracks) begin to appear on the surface of both specimens. The AE signal strength is significantly increased from LS2 to LS3 in load cycle 1. The sudden increase in AE signal strength corresponds to the formation of visible cracks. The same phenomenon was also observed by Md Nor et al. [32] where a sudden increase in AE signal strength corresponded to the first flexural crack due to fatigue loading.

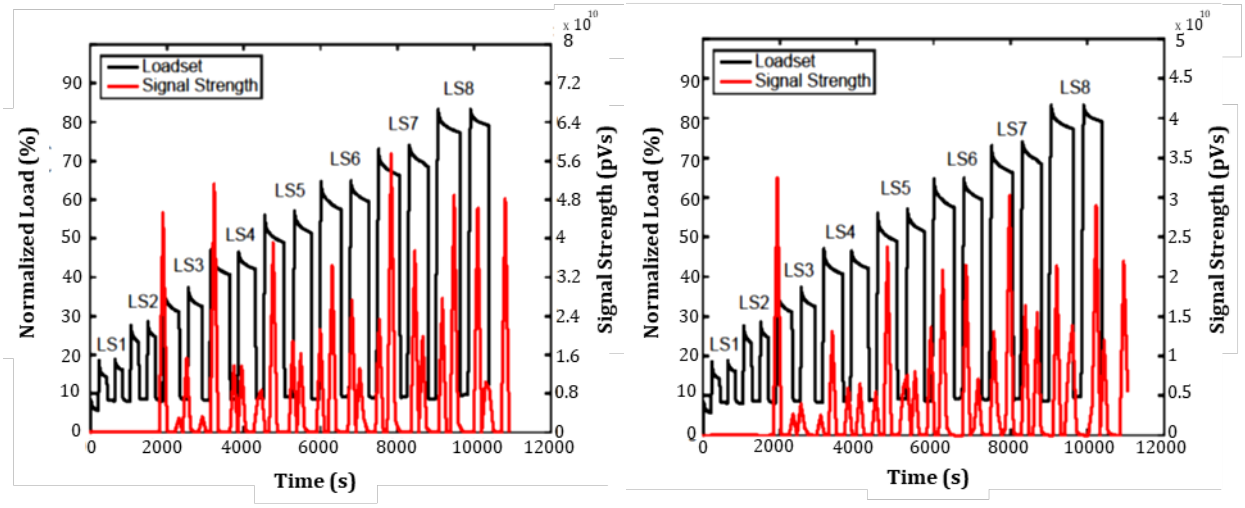

Fig. 7 *Normalized load, signal strength versus time for - (a) Specimen CTRL; and (b) Specimen CU-T45.*

At LS3, specimen CU-T45 recorded the highest value of signal strength at 3.246×10^{10} pVs, while 7 new cracks were formed under that load set, as shown in Fig. 7(b). This indicates that the AE signal strength correlates with the formation of visible cracks in the concrete specimen. Then, the signal strength value was decreased to 1.313×10^{10} pVs due to only 2 cracks observed at LS4. However, the value was increased to 2.375×10^{10} pVs at LS5. At this load set, the crack pattern begins to propagate diagonally towards the point of load application, and the signal strength for unloading in cycle 2 starts to become dominant.

At LS6, the signal strength value decreased to 2.085×10^{10} pVs with only 2 new shear cracks formed. However, both cycles for unloading recorded higher values compared to loading and reloading values. This phenomenon may be due to the transition of cracks from flexural to shear cracks in the shear region of the beam specimen. At LS7, 2 more shear cracks were formed in the shear region, and the value of signal strength was increased to

3.025×10^{10} pVs. The shear cracks were propagated beyond the neutral axis and intersected with flexural cracks towards the two-point load. The unloading value of signal strength was still dominant.

At the final load set, no new cracks were formed, and the existing shear cracks continued to propagate. Similarly, the flexural crack begins to propagate again towards the point of load application. In this load set, both cycle 1 and cycle 2 exhibited unloading dominance, indicating significant damage to the concrete specimen due to friction during crack closure. This finding was also reported by Elbatanouny et al. [22] showed that emission activity recorded during unloading on average is larger than emission activity during loading because of the crack closures, which result in friction between crack surfaces. Therefore, an increase in unloading emission activity can be considered as an indication of concrete cracking.

Comparing the CU-T45 specimen to the CTRL specimen, the AE signal strength in CTRL recorded a much higher value in LS3, LS4, LS5, LS7, and LS8. This is because the number of cracks produced in the CTRL specimen is higher compared to the CU-T45 specimen. The stress distribution within the beam specimen was reduced since the bonding between the steel reinforcement and concrete deteriorated due to the accumulation of corrosion products.

Fig. 8 shows the normalised load and cumulative signal strength versus time. The normalised load is the ratio between the applied loads at each phase and the ultimate load for the specimen. As can be seen from Fig. 8(a) and Fig. 8(b), the cumulative signal strength increased significantly at LS3 when the load was applied at 41% of the ultimate load. Based on visual inspection during the cyclic load test, visible cracks also appeared on the surface of the concrete at LS3. This suggests that the significant increase in cumulative signal strength can be used as an indicator of crack damage, as they correspond to each other. Patil et al. [33] found that significant rises in CSS, which is typically known as 'knee' in the CSS curve, may indicate damage to concrete due to cracking.

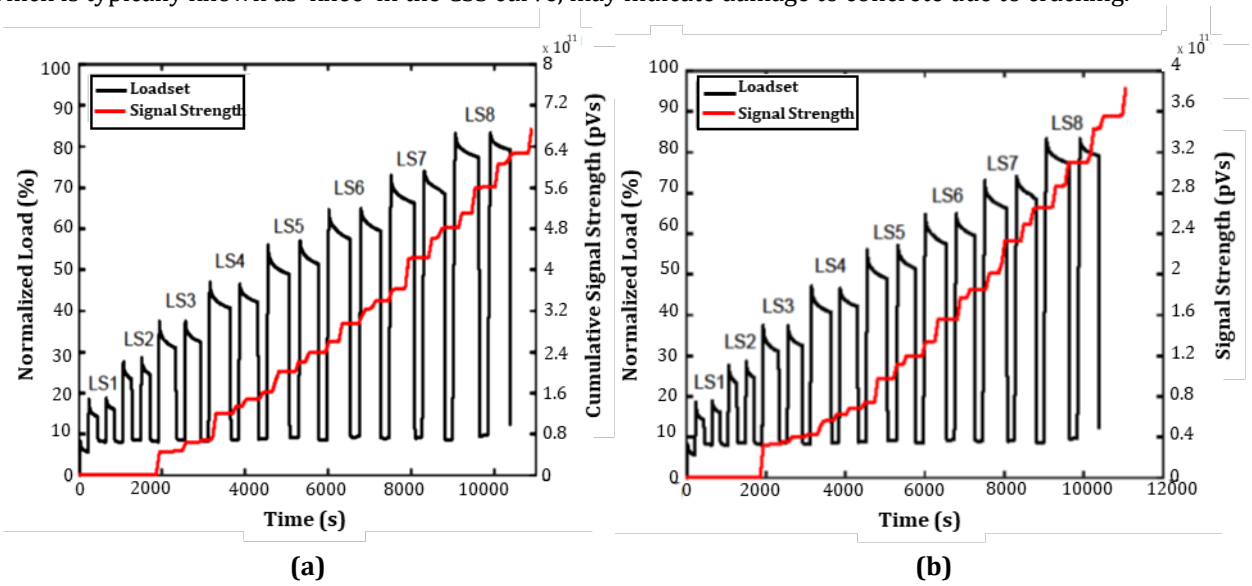

Fig. 8 *Normalised load, cumulative signal strength versus time for (a) Specimen CTRL; and (b) Specimen CU-T45*

For the CU-T45 specimen, all the visible cracks that appeared on the surface of the concrete were in the constant moment region, and some of them were propagated vertically beyond the neutral axis. Another significant increase in cumulative signal strength was in LS7, which produced the highest number of new shear cracks in the shear region. In this phase, the shear cracks have been propagated diagonally towards the two-point load. The LS8 recorded another significant increase in cumulative signal strength, which could be related to the propagation of shear cracks and also flexural cracks, even though no other cracks were formed. The accumulation of cracks from the beginning of the test until the final load set contributed to high signal strength due to friction from the crack's closures.

A summary can be made based on the trend of AE signal strength for each load set to identify the crack damage of the beam specimen under cyclic loading. The damage level can be associated with the formation of cracks at certain high signal strength values that correspond to the load set. The transition of cracks from the constant moment region to the shear region can also be used as an indicator of the damage level in the reinforced concrete specimen. Compared to the CTRL specimen, the cumulative signal strength recorded in this specimen showed a higher value than that of the CU-T45 specimen due to the number of cracks in the CTRL specimen being higher than that of CU-T45. Therefore, it can be inferred that the cumulative signal strength is a useful indicator for assessing damage to cracks in reinforced concrete structures.

Int. Journal of Integrated Engineering Vol. 17 No. 7 (2025) p. 274-286

3.3 CSS Unloading Ratio

The relationship between CSS and the reloading and unloading cycle of each load set is graphically shown in Fig. 9(a) and Fig. 9(b) for the CTRL and CU-T45 specimens, respectively. The CSS ratio (expressed in percentage) is presented over each unloading bar. The CSS of LS1 and LS2 were barely visible because the magnitude of CSS was relatively small in both specimens. On average, the CSS of both specimens increased gradually from the first load set to the final load set. The CSS significantly increased from LS2 to LS3, with a similar trend observed for both specimens. The significant increase in CSS corresponded to the first visible crack that appeared on the surface of the concrete specimen. According to Ohtsu [34], the AE activity during the unloading phase could be related to structural integrity. The structure is said to be statically stable when AE activity is rarely observed in the unloading phase. In contrast, when AE activity is highly observed during the unloading phase, the structure is statically unstable, and damage has accumulated within it.

The CTRL specimen became unloading dominant from LS4 to LS8, whereas the CU-T45 specimen became unloading dominant from LS5 to LS8. This finding was interesting because the CTRL specimen had the highest number of visible cracks, extending from LS4 to the final load set. The unloading became dominant because the AE activity increased primarily as a result of crack closure and friction during the unloading phase, compared with the reloading phase. As such, a high AE activity during unloading indicated great damage to the specimen. The number of visible cracks in the CU-T45 was smaller than that in the control specimen because the bonding between the steel reinforcement and the concrete had deteriorated due to the corrosion products. Therefore, the stresses generated during the test could not be transferred to the concrete, causing fewer cracks.

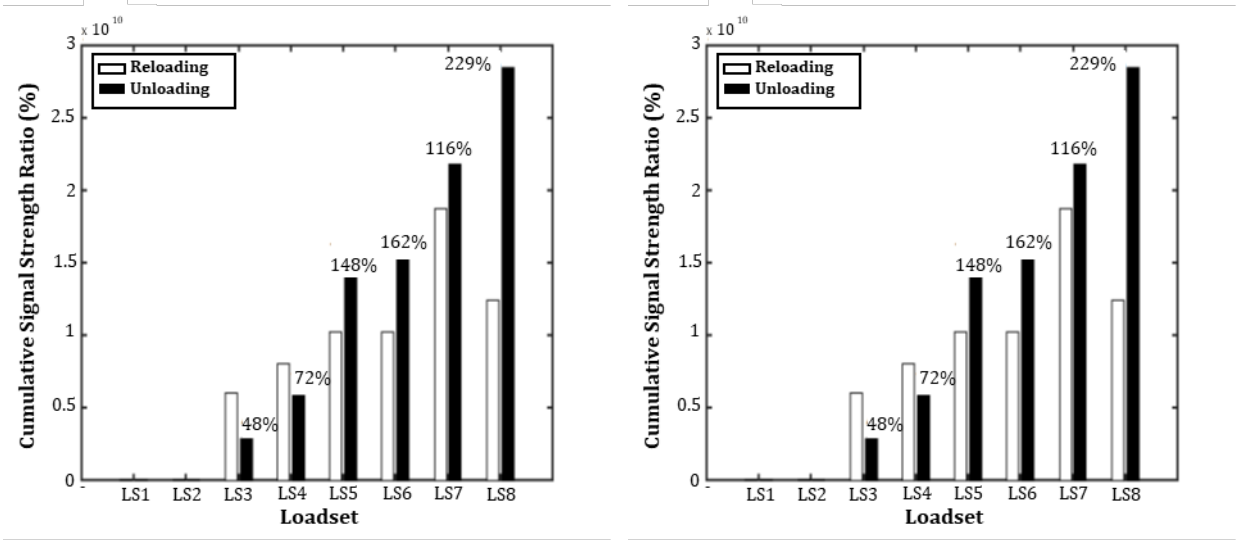

Fig. 9 *Cumulative signal strength versus load set for (a) Specimen CTRL; and (b) Specimen CU-T45*

4. Conclusion

In the presented study, the AE signal strength parameter data were used to evaluate the cracking behaviour and classify the crack damage of a corroded reinforced concrete beam subjected to repetitive loads of SCLT. The following conclusion can be drawn:

- The significant increase in signal strength confirms the association between the initiation and propagation of cracking in the reinforced concrete beam.
- The sudden increase in cumulative signal strength could be related to the transition of tensile cracks to shear cracks.
- The high AE signal strength during unloading compared to reloading indicates great damage to the specimen as a result of friction during the crack closure.
- The AE signal strength produced in the corroded specimen is lower compared to the control specimen due to less formation of visible cracks.

In summary, the results demonstrate that crack initiation and propagation in reinforced concrete beams are associated with increased signal strength, which significantly increases during the transition from tensile cracks to shear cracks. Additionally, fewer apparent cracks in corroded specimens result in a lower signal strength. Future research should look into the mechanics underlying cracking transitions and develop a more comprehensive AE-based corrosion monitoring technique.

Acknowledgement

The authors would like to thank the Ministry of Higher Education Malaysia for providing financial support under the Fundamental Research Grant Scheme (FRGS) No. FRGS/1/2022/TK06/UMP/02/1 (University reference RDU220101) and Faculty of Civil Engineering Technology, Universiti Malaysia Pahang Al-Sultan Abdullah for laboratory facilities.

Conflict of Interest

The authors declare that they have no conflict of interest regarding the publication of this paper.

Author Contribution

The authors confirm contribution to the paper as follows: ***Study conception and design:*** *Khairul Anuar Shahid, N. Muhammad Bunnori;* ***Data collection:*** *Khairul Anuar Shahid;* ***Analysis and interpretation of results:*** *Khairul Anuar Shahid, N. Muhammad Bunnori;* ***Draft manuscript preparation:*** *Khairul Anuar Shahid, Mohd Khairul Kamarudin. All authors reviewed the results and approved the final version of the manuscript.*

References

[1] Kementerian Kerja Raya (2007). JKR Kenal Pasti 400 Jambatan Kritikal. https://www.kkr.gov.my/ms/node/109970

[2] Wenzel, H. (2009). Health Monitoring of Bridges. John Wiley & Sons.

[3] Zaki, A., Chai, H., Aggelis, D., & Alver, N. (2015). Non-destructive evaluation for corrosion monitoring in concrete: A review and capability of acoustic emission technique. Sensors. https://doi.org/10.3390/s150819069

[4] ASTM E976-10 (2010). Standard Guide for Determining the Reproducibility of Acoustic Emission Sensor Response. ASTM International. https://doi.org/10.1520/E0976-10

[5] Liu, S., Pearson, M. R., Eaton, M., & Pullin, R. (2017). Correlation between acoustic emission distribution and stress variation through the depth of RC beam cross sections. Construction and Building Materials. https://doi.org/10.1016/j.conbuildmat.2017.06.001

[6] Geng, J., Sun, Q., Zhang, Y., Cao, L., & Zhang, W. (2017). Studying the dynamic damage failure of concrete based on acoustic emission. Construction and Building Materials. https://doi.org/10.1016/j.conbuildmat.2017.05.054

[7] Vidya Sagar, R. (2017). Acoustic emission characteristics of reinforced concrete beams with varying percentage of tension steel reinforcement under flexural loading. Case Studies in Construction Materials. https://doi.org/10.1016/j.cscm.2017.01.002

[8] Prem, P. R., & Murthy, A. R. (2017). Acoustic emission monitoring of reinforced concrete beams subjected to four-point-bending. Applied Acoustics. https://doi.org/10.1016/j.apacoust.2016.08.006

[9] Kaphle, M. (2012). Analysis of Acoustic Emission Data for Accurate Damage Assessment for Structural Health Monitoring. PhD Thesis. Queensland University of Technology.

[10] Webb, G. T., Vardanega, P. J., M., Fidler, P. R. A., Middleton, C. R., (2014). Analysis of structural health monitoring data from Hammersmith flyover. Journal of Bridge Engineering. https://doi.org/10.1061/(ASCE)BE.1943-5592.0000587

[11] ASTM E1316 (2011). Standard Terminology for Nondestructive Examinations. ASTM International. https://doi.org/10.1520/E1316-11B

[12] Ridge, A. R., & Ziehl, P. H. (2006). Evaluation of strengthened reinforced concrete beams: Cyclic load test and acoustic emission methods. ACI Structural Journal, 103, 832-841.

[13] Md Nor, N. (2014). Fatigue damage assessment of reinforced concrete beam using acoustic emission technique. PhD Thesis, Universiti Teknologi MARA.

[14] Mangual, J., Elbatanouny, M., Ziehl, P., & Matta, F. (2013). Corrosion damage quantification of prestressing strands using acoustic emission. Journal of Materials in Civil Engineering. https://doi.org/10.1061/(ASCE)MT.1943-5533.0000669

[15] Abouhussien, A. A., & Hassan, A. A. A. (2016). The use of acoustic emission intensity analysis for the assessment of cover crack growth in corroded concrete structures. Journal of Nondestructive Evaluation. https://doi.org/10.1007/s10921-016-0369-1

[16] Zaki, A., Kian, H., Behnia, A., Aggelis, D. G., Ying, J., & Ibrahim, Z. (2016). Monitoring fracture of steel corroded reinforced concrete members under flexure by acoustic emission technique. Construction and Building Materials. https://doi.org/10.1016/j.conbuildmat.2016.11.079

[17] Van Steen, C., Pahlavan, L., Wevers, M., & Verstrynge, E. (2019). Localisation and characterisation of corrosion damage in reinforced concrete by means of acoustic emission and X-ray computed tomography. Construction and Building Materials. https://doi.org/10.1016/j.conbuildmat.2018.11.159

[18] Wang, L., Yi, J., Xia, H., & Fan, L. (2016). Experimental study of a pull-out test of corroded steel and concrete using the acoustic emission monitoring method. Construction and Building Materials. https://doi.org/10.1016/j.conbuildmat.2016.06.046

[19] Eurocode 2 (2002). Design of Concrete Structures - Part 1. European Committee for Standardisation.

[20] Andrade, C., Alonso, C., & Molina, F. J. (1993). Cover cracking as a function of bar corrosion: Part I-experimental test. Materials and Structures. https://doi.org/10.1007/BF02472805

[21] ACI 437 (2012). Code Requirements for Load Testing of Existing Concrete Structures. American Concrete Institute

[22] Elbatanouny, M. K., Ziehl, P. H., Larosche, A., Mangual, J., Matta, F., & Nanni, A. (2014). Acoustic emission monitoring for assessment of prestressed concrete beams. Construction and Building Materials. https://doi.org/10.1016/j.conbuildmat.2014.01.100

[23] Liu, Z. (2007). Evaluation of Reinforced Concrete Beams Using Cyclic Load Test, Acoustic Emission, and Acousto-Ultrasonics. PhD Thesis, University of South Carolina.

[24] Shahidan, S., Pulin, R., Muhamad Bunnori, N., & Holford, K. M. (2013). Damage classification in reinforced concrete beam by acoustic emission signal analysis. Construction and Building Materials. https://doi.org/10.1016/j.conbuildmat.2013.03.095

[25] Md Nor, N., Ibrahim, A., Muhamad Bunnori, N., & Mohd Saman, H. (2013). Acoustic emission signal for fatigue crack classification on reinforced concrete beam. Construction and Building Materials. https://doi.org/10.1016/j.conbuildmat.2013.08.057

[26] Abdelrahman, M., ElBatanouny, M. K., & Ziehl, P. H. (2014). Acoustic emission based damage assessment method for prestressed concrete structures: Modified index of damage. Engineering Structures. https://doi.org/10.1016/j.engstruct.2013.12.037

[27] Md Nor, N., Ibrahim, A., Muhamad Bunnori, N., Saman, H. M., Mat Saliah, S. N., & Shahidan, S. (2014). Diagnostic of fatigue damage severity on reinforced concrete beam using acoustic emission technique. Engineering Failure Analysis. https://doi.org/10.1016/j.engfailanal.2013.07.015

[28] Mangual, J., ElBatanouny, M. K., Ziehl, P., & Matta, F. (2013). Acoustic-emission-based characterization of corrosion damage in cracked concrete with prestressing strand. ACI Materials Journal, 110, 89–98.

[29] McCormac, J. C., & Nelson, J. K. (2006). Design of Reinforced Concrete ACI 318-05 Code Edition. John Wiley & Sons.

[30] The Road Engineering Association of Malaysia (2000). A Guide for Bridge Inspection.

[31] Ou, Y. C., Susanto, Y. T. T., & Roh, H. (2016). Tensile behavior of naturally and artificially corroded steel bars. Construction and Building Materials. https://doi.org/10.1016/j.conbuildmat.2015.10.075

[32] Noorsuhada, M. N., Azmi, I., Norazura, M. B., Hamidah, M. S., Soffian Noor, M. S., & Shahiron, S. (2015). Fatigue crack inspection and acoustic emission characteristics of precast RC beam under repetition loading. Applied Mechanics and Materials. https://doi.org/10.4028/www.scientific.net/amm.773-774.1022

[33] Patil, S., Karkare, B., & Goyal, S. (2014). Acoustic emission vis-to-vis electrochemical techniques for corrosion monitoring of reinforced concrete element. Construction and Building Materials. https://doi.org/10.1016/j.conbuildmat.2014.06.068

[34] Ohtsu, M. (2015). Acoustic Emission (AE) and Related Evaluation (NDE) Techniques in the Fracture Mechanics of Concrete: Fundamentals and Application. Woodhead Publishing.